DEVELOPMENT OF A THREE-HOLE PROBE FOR UNSTEADY FLOW ANGLE MEASUREMENTS

D. Delhaye, G. Paniagua*, R. Dénos♣*

*Turbomachinery and Propulsion Department, von Karman Institute for Fluid Dynamics
Chaussée de Waterloo 72, B1640 – Rhode-Saint-Genèse, Belgium
delhaye@vki.ac.be, paniagua@vki.ac.be
♣Directorate-General for Research, European Commission
CDMA/04-137, B-1049 Brussels, Belgium

ABSTRACT

This contribution presents the development, calibration, and first application of a three-sensor directional fast response wedge probe at the VKI for aerodynamic measurements in turbomachines. The probe is equipped with flush-mounted standard fast response miniaturized pressure transducers. Angular calibrations were performed over a wide range of Mach numbers (0.3–0.7). A spectral analysis of the calibration tests together with CFD simulations were carried out to investigate the effects of the Reynolds and Mach numbers.

Tests were performed in the VKI compression tube HP turbine test rig at three pressure ratios ($P_{01}/P_{S3} = 2.4$, 3.8 & 5.1) at Reynolds = 10^6 based on the stator axial chord. Time-resolved angular measurements were obtained at high speed conditions (M_3 = 0.7) downstream of the rotor. The flow velocity was also measured at high frequency. The effects of the secondary flows were highlighted, and the rotor trailing edge shocks were identified. The data reduction was performed completely automatically, delivering the time-averaged and time-resolved angle, Mach, total and static pressures.

INTRODUCTION

In addition to contributing significantly to the cost of modern engines, the high pressure stages often determine the life of the gas turbine engine. The request of the industry for further decreases in specific fuel consumption and size has led to the development of single-stage HP turbines. Advanced highly loaded HP turbines are dominated by shock interactions due to the transonic flow regimes; hence, precise understanding of the complex three-dimensional unsteady flows is fundamental. Fast response instrumentation allows the measurement of the unsteady flow characteristics in flows with high turbulence levels and large pressure fluctuations. Fast response pressure probes provide unsteady static and total pressures, which allow the determination of the unsteady flow velocity. Despite the better signal-to-noise ratio of hot-wire anemometry, pressure based probes are extensively used in turbine testing because of their higher robustness and reliability.

The development and application of the fast response directional probe presented in this paper was driven by the testing of a transonic turbine stage in the von Karman Institute short duration facility (Sieverding & Arts, 1992). The main objective was the measurement of the time-resolved velocity vector, flow angle and pressure at the outlet of the turbine stage, where the blade passing frequency is of the order of 7 kHz.

The first attempts to develop fast response pressure probes correspond to the advent of piezoresistive pressure transducers in the early 1970's. The subsequent gradual decrease of the pressure sensors size then allowed the sensors to be placed accordingly closer to the sensing locations. The mounting of pressure transducers flush with the probe surface was pioneered by Kerrebrock et al. in 1974: a Ø 2.6 mm 3-sensor cylinder probe was developed for the MIT Blowdown Compressor Facility. The main advantages of the chip-on configuration are a high frequency response and the external mounting of the sensors onto the probe surface. This comes at the price of a relatively large pressure sensing area, and a direct exposure to dust particles and hot gas. Since then, several probe head geometries and sensor configurations have been investigated by many different authors, both in flush-mounted and sub-surface mounted transducers designs. The number of sensors reflects a compromise between probe size and the number of flow variables retrieved. Chip-on three-sensor wedge probes were developed Bubeck (1987), Cook (1989) and Cherret (1992). The respective effects of sensor location and wedge apex angle were studied by Humm et al., 1994, and Ainsworth, 1994, in large scale tests. The mounting of bare

piezoresistive sensing elements directly on the probe was investigated at Oxford by Ainsworth (1991) and at ETH Zurich by Gossweiler (1990). Recently, a sub-surface mounted chips design was experimented by Brouckaert, 2004, on a novel hybrid cylindrical/elliptical probe with trailing edge blowing for vortex street suppression.

NOMENCLATURE

Roman symbols:

A	[bar/V^2]	temperature sensitivity
B	[bar/V]	temperature offset
C	[bar/V]	temperature sensitivity
Cp	[deg.$^{-1}$]	Sensitivity coefficient
D	[bar]	temperature offset
d	[m]	characteristic length
f	[s^{-1}]	frequency
K	[-]	conditioning coefficient
l	[mm]	distance from sensor to apex
L	[mm]	length of wedge side
M	[-]	Mach number
P	[bar]	pressure
Re	[-]	Reynolds number = ρUd/μ
Str	[-]	Strouhal number = fd/U
U	[m/s]	velocity
V	[V]	voltage

Greek symbols:

α	[bar/V]	pressure sensitivity
β	[bar]	pressure offset
γ	[deg.]	extent of calibration range
μ	[kg/m.s]	dynamic viscosity
φ	[deg]	yaw angle
ρ	[kg/m^3]	density

Subscripts:

∞	far upstream
0	total value
atm	atmospheric
S	static value
C	central sensor
L	left sensor
R	right sensor
r	rotor frame of reference
1	stage inlet plane
3	stage outlet plane

PROBE DESIGN AND CALIBRATION

Head geometry

The fast response probe was designed to be used downstream of the ~0.8 m diameter VKI HP turbine stage. The choice of geometry and configuration is a compromise between many constraints. It was decided to use three sensors to retrieve both the angle of the flow in the blade to blade plane and the Mach number, while minimizing the probe head size to obtain a high special resolution and low blockage. The wedge geometry was chosen over cylindrical geometries for two main reasons:

- The wedge surfaces are flat and therefore well suited for the flush-mounting of commercial piezoelectric transducers. The chip-on design virtually eliminates the need to use a transfer function to recover the unsteady pressures.
- It is likely that large separations will be locked to the sharp rear angles of the probe, behind the lateral sensors (Ainsworth et al., 2000). On the contrary, Rodriguez (1984) and Brouckaert & Sieverding (1998) showed that cylindrical probes are particularly sensitive to unsteady wake induced perturbations.

Cook (1989) and Ainsworth (1994) showed that the angular sensitivity of wedge probes depends much more on the distance of the pressure sensor from the apex than on the wedge angle. The choice of the wedge angle is then a compromise between four constraints:

- minimize the disturbance of the flow,
- minimize the distance between the total pressure sensor and the yaw angle sensors to optimize spatial resolution,
- maximize the robustness of the probe,
- optimize the position of the lateral sensors to satisfy the sensitivity and calibration range requirements. Figure 1 shows these effects as measured by Humm et al., 1994.

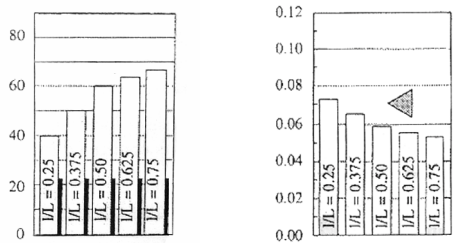

(a) (b)

Figure 1 (a) Calibration range ±γ [deg.] as a function of l/L the distance of the lateral sensor from the apex over the probe side length; (b) Sensitivity $\partial Cp/\partial\gamma$ [deg^{-1}] with $Cp=(P_L-P_R)/(\rho U_\infty/2)$. (Humm et al., 1994.)

The final apex included angle is 60 deg. with both sides measuring 3.5 mm. Two fast response Kulite® miniature pressure transducers (LQ-062-15A) were flush-mounted on the sides of the probe, close to the trailing edges. They are placed such that $l/L = 0.76$ with l calculated from the center of the sensors. A third sensor (XCQ-062-25A) is enclosed in a front-protruding cylinder of 1.65 mm diameter. The axis of the cylinder is radially displaced by 2.52 mm from the center of lateral sensors, to further decrease the dimensions of the probe and thus to increase its spatial resolution. A photo and 3D view of the probe together with a cut are shown in Figure 2. The absence of a pneumatic line or cavity between the

sensors and the flow allows measurements at high frequency (> 100 kHz) avoiding any spurious resonance effects. However, the direct exposure of the sensors to the flow makes the transducers vulnerable to the impact of particles.

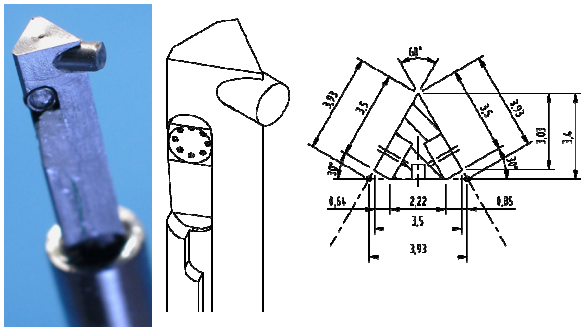

(a) (b) (c)

Figure 2 (a) Photo of the probe (b) 3D view of the probe; (c) Perpendicular cut at the level of the lateral sensors.

Static calibration

The miniature Kulite® pressure transducers are composed of a thin silicon membrane on the surface of which piezoresistors are mounted. The piezoresistors are sensitive to temperature hence post-test numerical compensation must be applied in tests performed in a fast transient temperature regime. Each sensor delivers two voltages: one is an image of the uncompensated pressure on the membrane and the other an image of the temperature of the piezoresistors. For each sensor, four coefficients are used in a bilinear law to recover the real pressure from the measured voltages:

$$P = \alpha V_{pressure} + \beta$$
$$\alpha = A V_{temperature} + B$$
$$\beta = C V_{temperature} + D$$

The coefficients are determined by an optimization routine which fits the sensor pressure to a low speed pneumatic probe recording, taking into account both voltages output by the transducer. The optimization objective of the fitting routine is the minimization of the sum of the absolute difference between the Kulite® sensor and the pneumatic recording at all sampling points. This method is described by Dénos, 2002. During angular calibration, the temperature was nearly constant. A linear law was therefore used for simplification. The slope of the calibration law was determined by measuring an average $V_{pressure}$ at atmospheric pressure and at near vacuum (17.5 mbar).

Angular calibration

The aerodynamic calibration of the probe was performed in the newly built vertical-nozzle free jet facility C4 of the von Karman Institute. The accuracy in the angle calibration was better than ± 0.15 deg. The sampling frequency was set at 100 Hz while the probe rotates step by step. The angular calibration was performed as a function of the yaw angle, at Mach numbers spanning from 0.3 to 0.7 in increments of 0.1. Acquisitions were performed from -50 to 50 deg. but only the range from -36 to 40 deg. was retained because strong gradients appeared in the calibration maps near the edges of the domain. Particular care was taken to avoid electric noise by switching off all unused electric equipment close to the facility.

The sensitivity of the aerodynamic calibration to the Reynolds number was assessed through 2D numerical simulations. Moreover, Dominy & Hodson (1992) showed that the flush-mounting of the sensors suppresses the increase in Reynolds number dependency typically caused by cavities between the sensors and the flow.

The evaluation of each aerodynamic variable of interest requires the definition of an associated non-dimensional calibration coefficient. To retrieve the velocity vector as well as both the static and the total pressures, four coefficients are therefore chosen:

$$K_{yaw}(\varphi, M) = \frac{P_L - P_R}{KP_C - \frac{(P_L + P_R)}{2}}$$

$$K_{Mach}(\varphi, M) = \frac{P_C}{KP_C - \frac{(P_L + P_R)}{2}}$$

$$K_{tot}(\varphi, M) = \frac{P_{tot} - P_C}{KP_C - \frac{(P_L + P_R)}{2}}$$

$$K_{dyn}(\varphi, M) = \frac{P_{tot} - P_{stat}}{KP_C - \frac{(P_L + P_R)}{2}}$$

The coefficients are modified versions of the ones proposed by Krause & Dudzinski (1969) (K_{yaw}, K_{tot}, and K_{dyn}) and Brouckaert (2004) (K_{Mach}). The modification consists in the addition of a constant multiplication factor K, to artificially increase the output of the central sensor. This factor is necessary for the calibration curves of the probe to follow a monotonous and quasi-linear evolution. The main advantage of this set of coefficients is the dependency of K_{yaw} and K_{Mach} solely on the sensors readings. From the calibration measurements, two-dimensional contour plots of the coefficients are created by bilinear interpolation (see Figure 3).

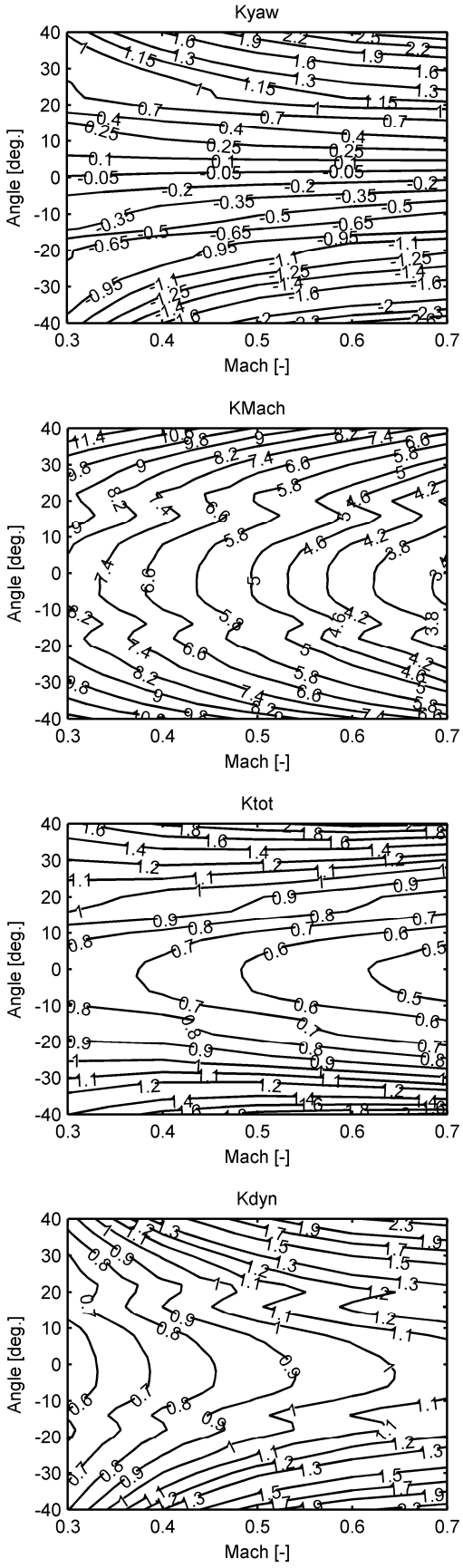

Figure 3 Calibration maps of the VKI 3-sensor probe.

The algorithm used to retrieve the aerodynamic variables of the flow is illustrated in Figure 4. For any given measurement, K_{yaw} and K_{Mach} are calculated. The algorithm then searches their associated 2D contour plots to find corresponding cells in which both the experimental K_{yaw} and K_{Mach} are contained. A bilinear subgrid is then laid on the selected cells and the same process is repeated. The angle and Mach number values are finally taken as the mean values of the corresponding subcells. The total and static pressures are then retrieved from the other two contour plots, using the angle and the Mach number. Note that, for this algorithm to yield a single value of angle and Mach number, the map of K_{yaw} must be monotonous in the direction of increasing yaw, and the map of K_{Mach} must be monotonous in the direction of increasing Mach.

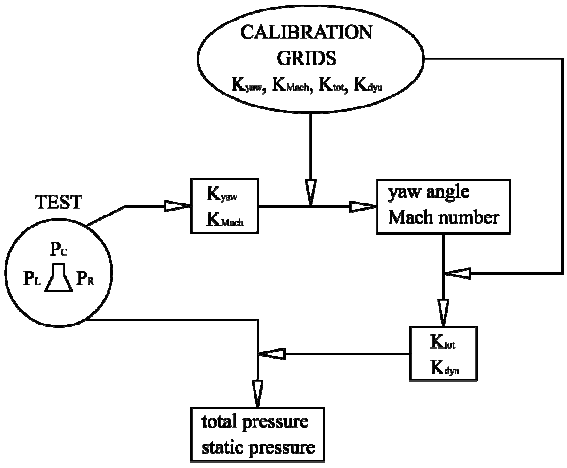

Figure 4 Data evaluation flow chart.

Calibration uncertainty

A detailed analysis of the measurement chain clearly indicated that the uncertainty on the Mach number is attributed mostly to the relative pressure transducer, which measures the upstream total pressure. Since the uncertainty of the transducer is independent of the pressure level, the largest uncertainty on the Mach number is obtained for the lowest velocity. At Mach 0.3, the uncertainty is 3.18% (20:1), whereas at Mach 0.7 it is of only 0.45% (20:1). The uncertainty on the yaw angle in the calibration facility is smaller than 0.15 deg. The maximum uncertainty on the Reynolds is 1.9% (20:1) at Mach 0.3.

The angular calibration was done twice to check its repeatability. The maximum difference between the curves was 1.15% of the total pressure. The difference between the pressure curves could be linked to the temperature variation of the gas of the calibration facility after successive runs. Indeed, the temperature of the blown air decreases during the blowdown.

Spectral analysis

An intense resonance frequency was identified in both the calibration and the turbine test data. It is locked to the first or second harmonic of the main upstream excitation. In the case of the calibration, the resonance appears around 6.5 kHz (see Figure 5-right), which is twice the upstream spurious pressure fluctuation (~ 3.25 kHz) represented in Figure 5-left. Figure 6 shows that its amplitude increases with the Mach number and that it appears around + 20 deg. on the right sensor and around - 20 and 0 deg. on the left sensor. Note that the +/- 20 deg. yaw angles correspond to the flow transitions which can be seen in Figure 10.

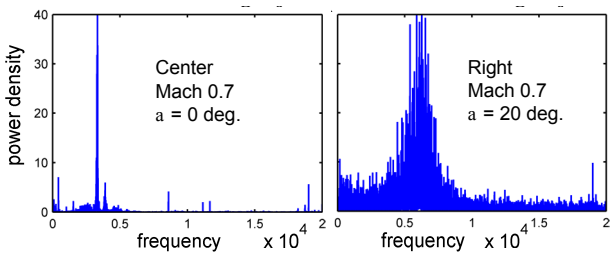

Figure 5 FFT of the raw sensor signals.

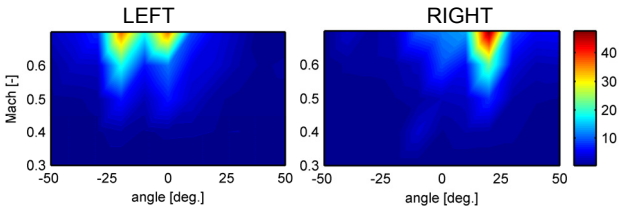

Figure 6 Intensity (PSD) of the resonance

In the turbine, the main upstream excitation is the blade passing frequency at ~ 7 kHz. Close to the hub wall, the resonance appears at ~ 14 kHz on the left sensor and ~ 21 kHz on the right sensor (see Figure 7), regardless of the operating conditions.

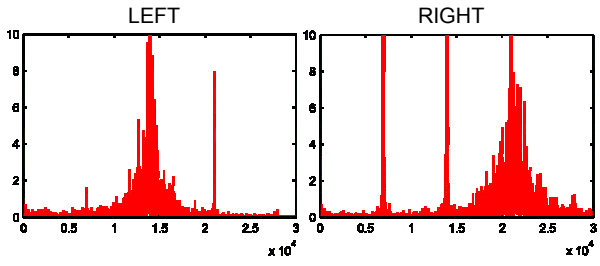

Figure 7 FFT of the raw sensor signals.

The fluctuating pressure phenomenon is probably due to the vortex shedding downstream of the probe, possibly in conjunction with an interaction with the recirculation bubble which originates at the probe apex.

NUMERICAL SIMULATIONS

Wake induced perturbations

Two-dimensional numerical simulations were performed with Fluent® on a transverse cut of the probe head at the level of the lateral sensors (see Figure 2-c) to investigate the effect of wake induced perturbations and other periodic phenomena. A segregated solver was used with a k-epsilon viscosity model. The time discretisation was second-order implicit with a time step of 10^{-6} s. The unstructured triangular mesh of 150.000 elements was refined close the probe surface to capture the boundary layer.

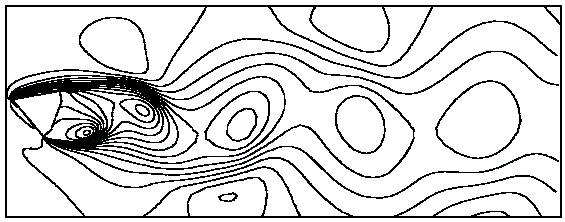

Figure 8 Total pressure contours at Mach 0.7 and a yaw angle of 20 deg.

With the same conditions than that found in the calibration facility, the isopressure lines show that the large separations are locked to the sharp rear corners of the probe (see Figure 8) as described by Ainsworth et al., 2000. Vortices are shed alternatively from the two sides of the probe and induce pressure fluctuations on the lateral sensors. The effect of these fluctuations on the angular reading of the probe is influenced by their amplitude and relative phase. Table 1 summarizes the effect of the downstream vortex shedding for the different angles. The angular fluctuations measured by the virtual probe are important, reaching 6.02 deg. at a yaw angle of 20 deg. The low fluctuation (0.65 deg.) found at 30 deg. are explained by the lateral pressure fluctuations being nearly in phase. The decrease in vortex shedding frequency associated with the increase in angle is explained by the diminishing size of the area of the probe facing the flow orthogonally. Considering a characteristic dimension (see Figure 2-c) of 3.5 mm (resp. 3.93), the Strouhal number at zero degree is 0.175 (resp. 0.196).

Yaw angle [deg.]	0	+20	+30
Left pressure fluctuations [mbar]	31.4	35.4	11.1
Right pressure fluctuations [mbar]	31.4	73.4	43.1
Yaw angle fluctuation [deg.]	3.70	6.02	0.65
Fluctuations frequency [kHz]	11.49	11.12	9.17

Table 1 Wake induced perturbations at Mach 0.7 and P_{atm}, as a function of the angle.

Recirculation bubble

The numerical simulations show the presence of a recirculation bubble close to the apex of the probe when the probe is placed at a non-zero

yaw angle. At Mach 0.7, atmospheric pressure, and at a yaw angle of 20 deg., it is however of limited size: it extends from the apex to l/L ≈ 0.185 (see Figure 10-a). At 30 deg., the recirculation covers nearly the whole side of the probe ($l/L = 0.87$) (see Figure 10-b).

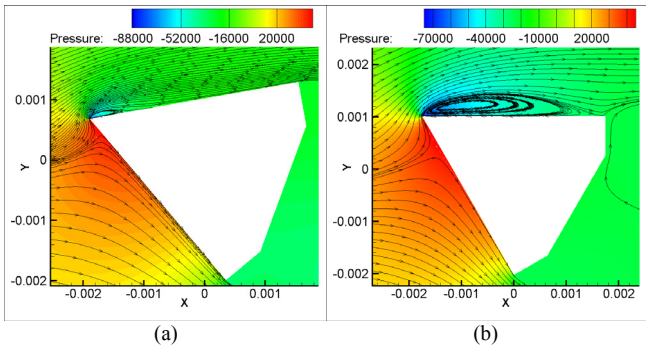

(a) (b)

Figure 9 Snapshots of the recirculation bubble which extends from apex to (a) $l/L \approx 0.185$ at 20 deg.; (b) $l/L \approx 0.87$ at 30 deg

The experimental pressure recordings of the calibration curves seem however to indicate that the recirculation influences the lateral sensors from ~±20 deg at all Mach numbers (see Figure 10). This discrepancy could be caused by the influence of the front protruding cylinder on the flow.

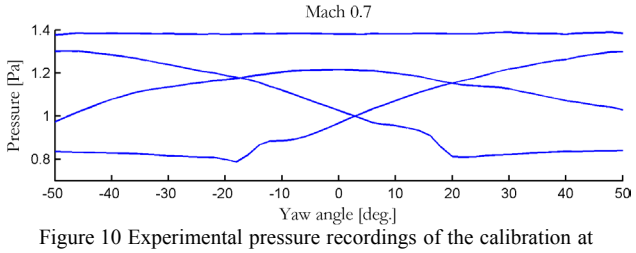

Figure 10 Experimental pressure recordings of the calibration at Mach 0.7.

Influence of the Reynolds

The effect of the Reynolds number on the probe readings is of particular importance because the calibration was performed at atmospheric pressure whereas the static pressure downstream of the turbine is roughly half that value. At Re = 23000, the size of the recirculation bubble is only marginally different than at atmospheric condition (Re = 47000): it extends from apex to $l/L = 0.158$ at 20 deg. yaw angle and $l/L = 0.96$ at 30 deg. The mean pressures on the lateral sensors are virtually identical at 0 and 30 deg. but yield a 27% difference on Kyaw at 20 deg.; this translates into an error on the yaw angle of 6.4 deg. Figure 11 shows the calibration curve at Mach 0.7, as well as the CFD calibration points: black circles for atmospheric conditions, red crosses for turbine conditions.

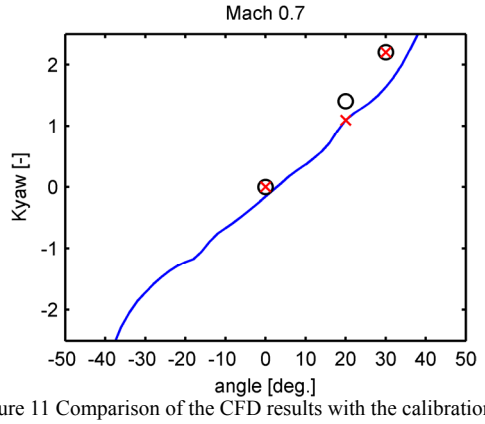

Figure 11 Comparison of the CFD results with the calibration.

TURBINE MEASUREMENTS

Turbine test rig and conditions

The turbine measurements were performed in the VKI compression tube turbine test rig CT3. The test section of the facility consists of a full transonic turbine stage, fed with air by a compression tube based on Oxford's "Isentropic Light Piston Compression Tube" concept. Its outlet is connected to a dump tank by a duct equipped with a sonic throat which allows the adjustment of the downstream static pressure. This setup is capable of simulating both the pressure ratio and the operating Reynolds number found in real engines.

All tests were performed at nominal rotor speed (6500 RPM) for a single Reynolds number (~1.065×10^6 based on the stator blades chord) and three different pressure ratios. Table 2 summarizes the turbine tests conditions.

Pressure ratio	P_{01}/P_{03} [-]	P_{01}/P_{S3} [-]	P_{S3} [bar]	M_{3r} [-]
Low	2.19	2.4	~0.68	0.65
Nominal	3.19	3.8	~0.43	0.97
High	3.85	5.1	~0.32	1.18

Table 2 Turbine tests conditions.

The probe was placed downstream of the rotor at different spans. The axis of the probe was situated at 18.4 mm from the plane defined by the tips of the trailing edges of the blades of the rotor (see Figure 12).

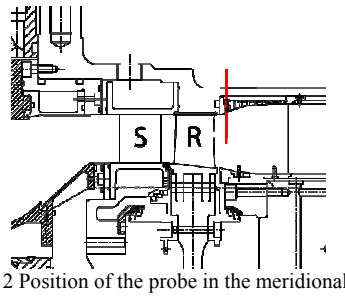

Figure 12 Position of the probe in the meridional plane.

The output of the probe was split in two: an unamplified low pass filtered signal (at 750 Hz), and an amplified high pass filtered signal (at 100 Hz) sampled at 300 kHz. The first was used for time-averaged measurements and the second for time-resolved measurements.

Phase-Locked Averaging

In addition to time-averaged measurements, the VKI fast response directional probe provides time-resolved measurements. Downstream of the turbine rotor, the flow follows a periodic evolution at the blade passing frequency. For this reason, an interesting way to describe the flow behavior is to retrieve the aerodynamic variables from the Phase-Locked Averaged pressures. These are computed by isolating a number of blade passages, dividing them into a fixed number of "classes", and making averages among the corresponding classes. Figure 13 illustrates the principle of phase-locking. The number of classes is chosen as the number of samples recorded per blade passing event. The evolution of the flow is then plotted as a function of the "phase". The zero phase ($\Phi = 0$) is defined as the position in which the stacking axis of the blades is directly in front of the sensor. The phase is equal to 1 after the rotor has completed one rotor pitch displacement (see Figure 14-a). It is important to note that the recordings of the three sensors of the probe are time-synchronized but not phase-synchronized because the sensors are not exactly in the same angular position. A correction is therefore needed. Figure 14-b shows the simplified head geometry used to apply the phase correction.

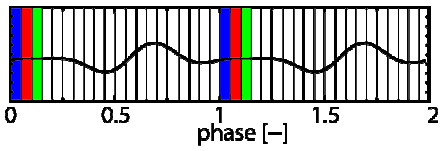

Figure 13 Corresponding classes for the Phase-Locked Averaging.

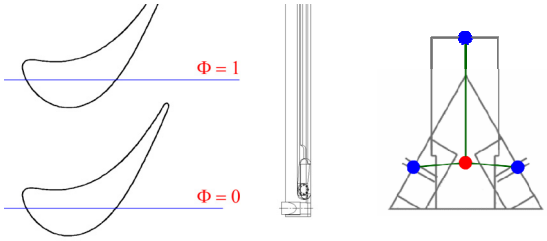

(a) (b)

Figure 14 (a) Phase-locking: one rotor pitch; (b) Simplified head geometry.

Measurements

The probe provides both time-averaged and time-resolved results. Comparison of the steady measurements with pneumatic recordings has shown good agreement. Figure 15 illustrates the time evolution of the rotor outlet flow angle during a typical test at the three pressure ratios, as well as the time-averaged angle as a function of span; the red curve corresponds to NISRE estimates. The effect of the secondary flows can be clearly identified. Note that the downward trend of the angle during the tests is caused by the acceleration of the rotor.

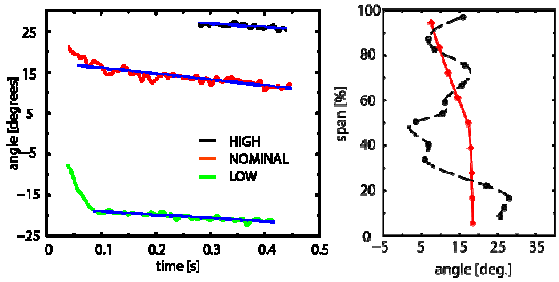

(a) (b)

Figure 15 Rotor outlet angle: (a) time-resolved; (b) time-averaged.

The PLA of the central sensor pressure at midspan under high pressure ratio is shown in Figure 16. Large fluctuations of amplitude 6% of P_{01} are observed at phase 0.6; they correspond to the passing of the rotor blades trailing edge shock. The lines above and below the pressure curves correspond to the addition and the subtraction of the RMS to the PLA; this indicates the time-unresolved component.

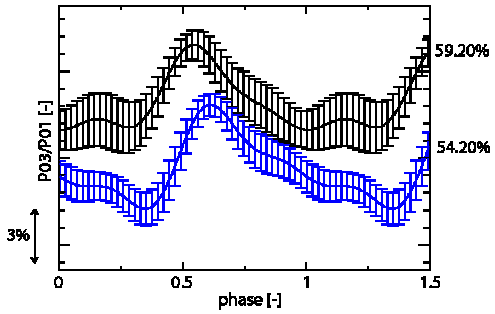

Figure 16 Pressure PLA and RMS at midspan under high pressure ratio.

The colormaps of Figure 17 show the PLA of the angle variation (with respect to the pitchwise mean values) and the Mach at the low pressure ratio. Angular fluctuations of 16 deg. are observed across a pitch at 86 % span; they are caused by the tip clearance vortex which is driven by a jet of hot gas that leaks from the pressure side towards the suction side of the rotor blade, mostly in the trailing edge region (Heider et al, 1993). The underturning associated to the passage vortex can also be seen from 25 to 60 % span; it fluctuates between -5 and +7 deg. around the mean pitchwise angles.

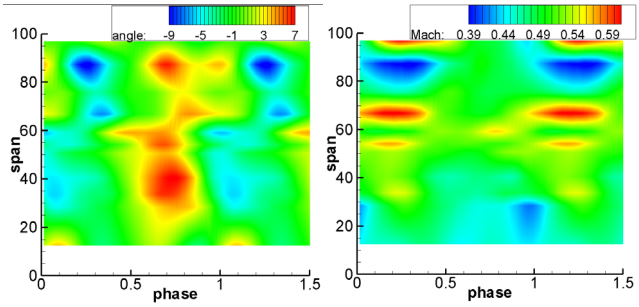

Figure 17 PLA of the angle variation and Mach at the low pressure ratio.

CONCLUSIONS

Fast response aerodynamic probes have become an essential tool in the study of the flow field in turbomachines thanks to their ability to measure both the steady and unsteady components of the flow vector as well as the total and static pressures.

The accuracy of the measurements depends on many different factors. The requirements of the turbine test rig have led to the choice of a wedge shaped probe head with a 60 deg. apex angle: it exhibits a large calibration range with good dynamic characteristics. Indeed, unsteady errors are reduced by the absence of cavity resonance and the limited effect of vortex interaction downstream of the probe. Still, both an extensive angular calibration and a careful sensor calibration are needed.

Numerical simulations show that the large separation at the rear of the probe has little influence on the flow over the lateral sensors, and that the recirculation bubble remains of small size from 0 to 20 deg. yaw angle. Also, the numerical results indicate that the calibration at atmospheric pressure is valid for the turbine measurements, roughly at half the static pressure. The unsteady separation bubble is probably triggered by the unsteady flows.

The present study has provided steady and unsteady measurements downstream of the turbine stage. The influence of the secondary flows was assessed and the presence of shocks identified downstream of the stage. Designers can profit from a better understanding of unsteady flow physics and achieve improvement in the turbine design. Furthermore, the contribution of this work to the knowledge in the behavior of fast response probes will facilitate the development of future measurement tools.

ACKNOWLEDGMENTS

The authors wish to acknowledge the contributions to this work of T. Yasa, G. Persico, and B. Adiloglu. The authors would also like to acknowledge the financial support of the European Commission and European manufacturers that are participating to the Project TATEF2 “Turbine Aero-Thermal External Flows 2”.

REFERENCES

Ainsworth R.W., Allen J.L., Batt J.J.M., 1994: “The Development of Fast Response Aerodynamic Probes for Flow Measurements in Turbomachinery”, *ASME Paper 94-GT-23*. The Hague, Netherlands.

Ainsworth R.W., Dietz A.J., Nunn T.A., 1991: “The Use of Semiconductor Sensors for Blade Surface Pressure Measurements”, *Journal of Engineering for Gas Turbines and Power, Vol. 113*.

Ainsworth R. W., Miller R. J., Moss R. W., Thorpe S. J., 2000: “Unsteady pressure measurement”, *Measurement Science and Technology 11 (2000),* University of Oxford, Department of Engineering Science, Oxford, UK.

Brouckaert J.-F., 2004: “Development of Fast Response Aerodynamic Pressure Probes for Time-Resolved Measurements in Turbomachines”. *Ph.D. Thesis*. von Karman Institute for Fluid Dynamics. Brussels, Belgium. ISBN 2-930389-08-7.

Brouckaert J.-F., Sieverding, C.H.; Manna M., 1998, “Development of fast response 3-hole pressure probe”. *Proceedings of the 14th Symposium on Measuring Techniques for Transonic and Supersonic Flows in Cascades and Turbomachines.* Limerick, Ireland.

Bubeck H., 1987: “Entwicklung einer Keilsonde zur dreidimensionalen instationären Strömungsmessung und deren Anwendung in einem Axialverdichter”, *Mitteilungen des Institutes für Thermische Strömungsmaschinen und Maschinenlaboratorium der Universität Stuttgart (Nr. 27)*. Germany.

Cherret M.P., 1992: “Temperature error compensation applied to pressure measurements taken with miniature semi-conductors pressure transducers in a high speed research compressor”. *Proceedings of the 11th Symposium on Measuring Techniques for Transonic and Supersonic Flow in Cascades and Turbomachines.* München.

Cook, S.C.P., 1989: “The Development of a High Response Aerodynamic Wedge Probe and Use on High-Speed Research Compressor”, *Proceedings of the 9th Symposium on Air Breathing Engines. ISABE 89-7118. Athens.*

Dénos R., 2002: “Influence of Temperature Transients and Centrifugal Force on Fast Response Pressure Transducers”. *Experiments in fluids. Volume 33, Issue 2, pp 256-264.*

Dominy R.G., Hodson H.P., 1992: “An investigation of factors influencing the calibration of 5-hole probes for 3-D flow measurement”. *ASME Paper 92-GT 216*.

Gossweiler C., Humm H.J., Kupferschmied P., 1990: "The use of piezoresistive pressure transducers for fast response pressure measurements in turbomachinery", *Proceedings of the 10th Symposium on Measuring Techniques for Transonic and Supersonic Flow in Cascades and Turbomachines*, von Karman Institute. Belgium.

Heider R., Duboué J.M., Petot B., Billonet G., Couiller V. and Liamis N., 1993: "Three-Dimensional Analysis of Turbine Rotor Flow Including Tip Clearance". *ASME Paper*: 93-GT-111.

Humm H.J., Gossweiler C., Gyamarthy G., 1994: "On fast response probes: Part 2 – Aerodynamic probe design studies". *ASME Paper 94-GT-27*. The Hague, Netherlands.

Kerrebrock J.L., Epstein A.H., Haines D.M., Thompkins W.T., 1974: "The MIT Blowdown Compressor Facility", *Journal of Engineering for Power, Transactions of ASME Series A, Vol. 46 (Nr.4)*.

Krause L. N. and Dudzinski T. J., 1969: "Flow-direction Measurement with Fixed Position Probes in Subsonic Flow over a Range of Reynolds Numbers", *Proceedings of the 15th Int. ISA Aerospace Instrumentation Symposium*. Las Vegas, United States of America.

Rodriguez O., 1984: "The circular cylinder in subsonic and transonic flow", *AIAA Journal, Vol. 22, No 12*.

Sieverding C.H., Arts T., 1992: "The VKI compression tube annular cascade facility CT-3", *ASME Paper 92-GT-336*.